FERMILAB-TM-2301-E

Mechanical Properties of D0 Run IIB Silicon Detector Staves

Giobatta Lanfranco and James Fast

Fermi National Accelerator Laboratory
Particle Physics Division /Mechanical Dep. - Silicon Engineering Group
e-mail: giobatta@fnal.gov, jfast@fnal.gov

14 June 2001

1. Abstract

A proposed stave design for the D0 Run IIb silicon tracker outer layers featuring central cooling channels and a composite shell mechanical structure is evaluated for self-deflection and deflection due to external loads. This paper contains an introduction to the stave structure, a section devoted to composite lamina and laminate properties and finally a section discussing the beam deflections expected for assembled staves using these laminates.

2. The stave design

The outermost layers of the detector are formed by twelve silicon sensors, 37.2 mm wide by 100 mm long, glued together into 1.2 m chains with readout electronics (hybrids) glued to the top surface. The spacing of the hybrids along the 1.2 m stave length is still under discussion, but is not critical to the mechanical studies presented in this paper. The stave is assembled starting from a central core consisting of three Rohacell foam (or other core material) strips interspersed with a pair of PEEK (or aluminum) cooling tubes. A thin (0.10-0.2 mm) surface ply of carbon fiber (or perhaps Kapton or pyrolitic graphite sheet) is adhesive bonded to the core material and cooling lines, as well as reinforced mounting points at the ends of the staves. These skins are primarily used for thermal management and are not included in the finite element analyses (FEA) presented below. The 1.2 m long silicon chains are bonded to either side of the core with axial strip readout on one side and small angle stereo strip readout on the other. Finally, two composite C-channels are attached around the silicon to form a box structure that provides most of the stave stiffness. An end-view of a stave is shown in Figure 1. The stave length is 48” (1.22m) with support provided at the center and the two ends. None of the supports

are thought to provide a moment connection. We have also studied simple supports at only the ends of the staves, as this may be representative of the support condition at some stages of assembly.

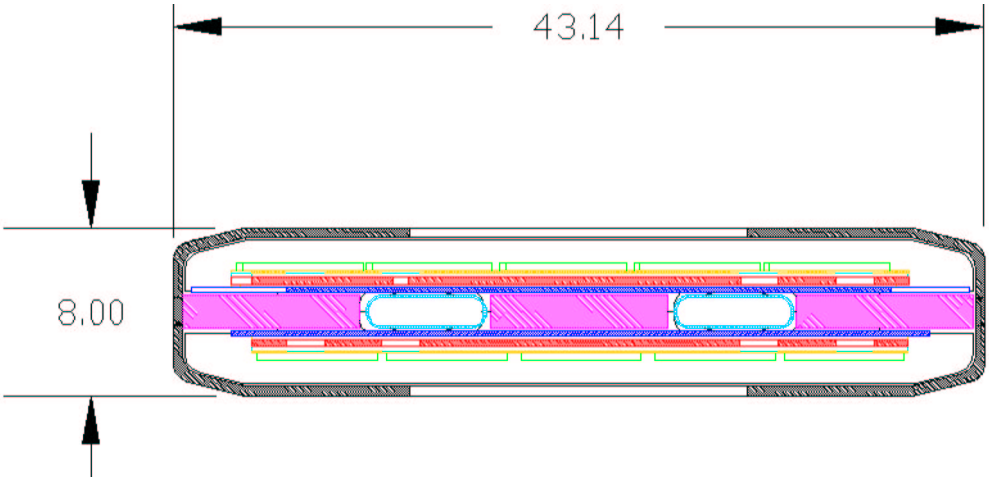

Figure 1 – The ladder section

Component	Material	Thickness [μm]	Color in Figure 1
Support Shell	Carbon Fiber	500	black
Sensor	Silicon	300	blue
Chip	Silicon	380	green
Glue	Epoxy	50	white
Core	Rohacell	2000	magenta
Tubing	PEEK	100 (wall thickness)	cyan
Heat spreader	Carbon Fiber	100 (3 plies x 33 μm)	not shown
HDI	Kapton	100	gold
Substrate	BeO	500	red

Table 1 – Stave constituent materials

3. Development of laminate properties

3.1. Introduction

The design of a silicon tracker stave must balance different requirements: providing a stiff, stable structural support for the silicon sensors, sufficiently matching the coefficient of thermal expansion of the silicon sensors in order to avoid thermal bowing and stress, limiting the amount of material so that multiple scattering will not affect the precision of the detector. The latter requirement is of much greater importance between the collision point and the second measurement point, however generation of secondaries (e.g. from photon conversions) is an issue throughout the detector volume.

This section presents a satisfactory carbon fiber lay-up and its performance; the results will be used in the following section to carry out a theoretical mechanical analysis of the present D0 stave design in order to verify its structural feasibility.

In order to meet both the mechanical stiffness requirements and the desired thermal expansion for the composites, previous ladder rails for D0 and CDF have utilized Hybor, a boron/carbon mix manufactured by Textron. Boron fiber is produced by chemical vapor deposition on a tungsten wire substrate. Although in the past Textron produced some boron fibers on a carbon fiber substrate, due to production difficulties the boron fiber is only available with a tungsten wire core at this time. The result is a composite with a relatively low radiation length, about 13cm vs. 25cm for a carbon fiber laminate.

3.2. Laminae and laminate properties

The laminae are the individual plies of fiber pre-impregnated with resin used to build up composite laminates (plates or structures).

Table 2 and

Table 3 summarize the physical properties of the boron and carbon laminae used in this study.

Table 4,

Table 5 and Table 6 contain the laminate lay-up and theoretical laminate properties for three possible laminae configurations that closely match the CTE of silicon. The first and third use both boron and carbon while the second uses only carbon. For a carbon only laminate the fibers cannot be oriented along the longitudinal direction or the CTE will be reduced to near 0. The result is that the longitudinal stiffness, E_x, of the carbon-only lay-up is about ¼ that of the carbon/boron mix. This lay-up is

considered for sections of the stave shell that are involved only in carrying shear and which will be largely cut away to reduce mass, rendering longitudinal fibers in these regions ineffective.

Boron 5505/4

E1	186.2 Gpa
E2	18.6 Gpa
E3	18.6 Gpa
G12	6.2 Gpa
G13	0.1 Gpa
G23	0.1 Gpa
NU12	0.21
NU13	0.21
NU23	0.41
CTE1	3.06E-06 mm/mm/C
CTE2	2.36E-05 mm/mm/C
CTE3	2.36E-05 mm/mm/C
E1	6.55E-03 mm/mm
E2	4.10E-03 mm/mm
E12	1.48E-02 mm/mm
E1	-1.25E-04 mm/mm
E2	-1.78E-04 mm/mm
E12	-1.48E-02 mm/mm
Density	2.01 g/cm³

Table 2- Physical properties of boron fiber prepreg

k139-1515-70/30

E1	424.7 GPa
E2	5.9 GPa
E3	5.9 GPa
G12	2.2 GPa
G13	2.2 GPa
G23	1.3 GPa
NU12	0.32
NU13	0.32
NU23	0.56
CTE1	-1.26E-06 mm/mm/C
CTE2	2.16E-05 mm/mm/C
CTE3	2.16E-05 mm/mm/C
E1	5.16E-03 mm/mm
E2	9.19E-02 mm/mm
E12	1.76E-02 mm/mm
E1	-1.36E-03 mm/mm
E2	-2.18E-02 mm/mm
E12	-1.76E-02 mm/mm
Density	1.71 g/cm³

Table 3 - Physical properties of carbon fiber prepreg

Boron 5505/4 + k139-1515-70/30

Ply #	Lamina Type	Thickness	Angle
1	k139-1515-70/30	55	54
2	Boron 5505/4	135	0
3	k139-1515-70/30	55	-54
4	k139-1515-70/30	55	-54
5	Boron 5505/4	135	0
6	k139-1515-70/30	55	54

Ex (pa)	106.2 GPa
Ey (pa)	77.5 GPa
Ez (pa)	15.7 GPa
Gxy (pa)	46.9 GPa
Gxz (pa)	0.8 GPa
Gyz (pa)	0.9 GPa
NUxy	0.49
NUyx	0.36
NUxz	0.14
NUzx	0.02
NUyz	0.31
NUzy	0.06
CTEx	2.50E-06 mm/mm/C
CTEy	1.03E-07 mm/mm/C
CTEz	3.31E-05 mm/mm/C
Density	1.875 g/cm³
Thickness	490 Micron

Table 4 – Lay-up and properties of the laminate containing boron

k139-1515-70/30

Ply #	Lamina Type	Thickness	Angle
1	k139-1515-70/30	80	90
2	k139-1515-70/30	80	53
3	k139-1515-70/30	80	-53
4	k139-1515-70/30	80	-53
5	k139-1515-70/30	80	53
6	k139-1515-70/30	80	90

Ex (pa)	25.7 GPa
Ey (pa)	156.3 GPa
Ez (pa)	8.1 GPa
Gxy (pa)	66.7 GPa
Gxz (pa)	1.5 GPa
Gyz (pa)	2.0 GPa
NUxy	0.26
NUyx	1.56
NUxz	0.42
NUzx	0.13
NUyz	-0.34
NUzy	-0.02
CTEx	2.47E-06 mm/mm/C
CTEy	-1.96E-06 mm/mm/C
CTEz	3.29E-05 mm/mm/C
Density	1.714 g/cm³
Thickness	480 micron

Table 5 - Lay-up and properties of the laminate containing only carbon fiber

Boron 5505/4 + k139-1515-70/30 - ALTERNATIVE

Ply #	Lamina Type	Thickness	Angle
1	Boron 5505/4	135	0
2	k139-1515-70/30	55	53
3	k139-1515-70/30	55	-53
4	k139-1515-70/30	55	-53
5	k139-1515-70/30	55	53
6	Boron 5505/4	135	0

Ex (pa)	106.5 GPa
Ey (pa)	73.1 GPa
Ez (pa)	15.7 GPa
Gxy (pa)	47.8 GPa
Gxz (pa)	0.8 GPa
Gyz (pa)	0.9 GPa
NUxy	0.52
NUyx	0.36
NUxz	0.13
NUzx	0.02
NUyz	0.31
NUzy	0.07
CTEx	2.39E-06 mm/mm/C
CTEy	1.91E-07 mm/mm/C
CTEz	3.31E-05 mm/mm/C
Density	1.875 g/cm³
Thickness	490 micron

Table 6 - Lay-up and properties of the alternative boron laminate

4. Deflections of stave structures

4.1. Structural configuration

Four different configurations for the laminate structure have been considered (Figure 2). The first configuration is a structure made with boron/carbon mix throughout the shell. This is not desirable from a radiation length standpoint due to the tungsten filaments in the boron fibers and from a fabrication standpoint as it will be very difficult to cut through the boron fibers to make the windows to bring cables out through. The second configuration is all carbon fiber. As mentioned above, the longitudinal stiffness of this lay-up is very low and the deflections are unacceptably large. The third configuration has boron/carbon mix in C-shaped regions on the two sides of the structure. These provide the longitudinal stiffness and allow the windows to be cut through pure carbon regions down the center of the structure. The forth configuration is very similar to the third, except that the boron has also been removed from the vertical (side) members to further reduce the mass. Analysis of the effects of large area windows cut in the C-channels are beyond the scope of this study and will require fabrication and load testing of prototype structures.

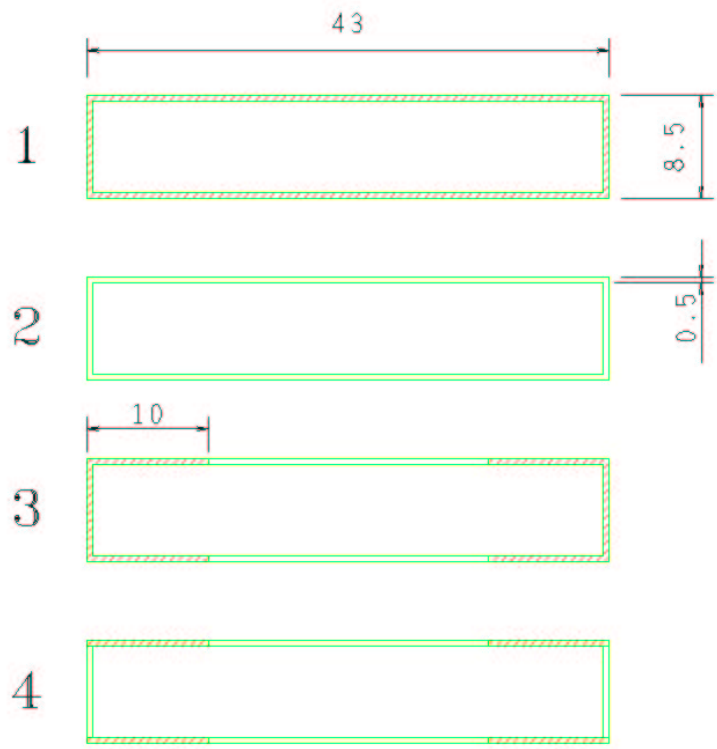

Figure 2 - Material Configurations (the Boron prepreg appears hatched). Dimensions in mm.

4.2. Analytical study

As a starting point the bending and torsional stiffness of the four shell configurations were calculated analytically. The results are presented in Figure 3. As expected the second configuration, which has only carbon fibers at large angles to the long axis of the stave, shows very low bending stiffness. The first case has the highest bending stiffness, but the material content required to achieve this would be unacceptable. The last two cases offer a reasonable balance between beam stiffness and material content and are representative of the objects that are envisioned for use in the detector.

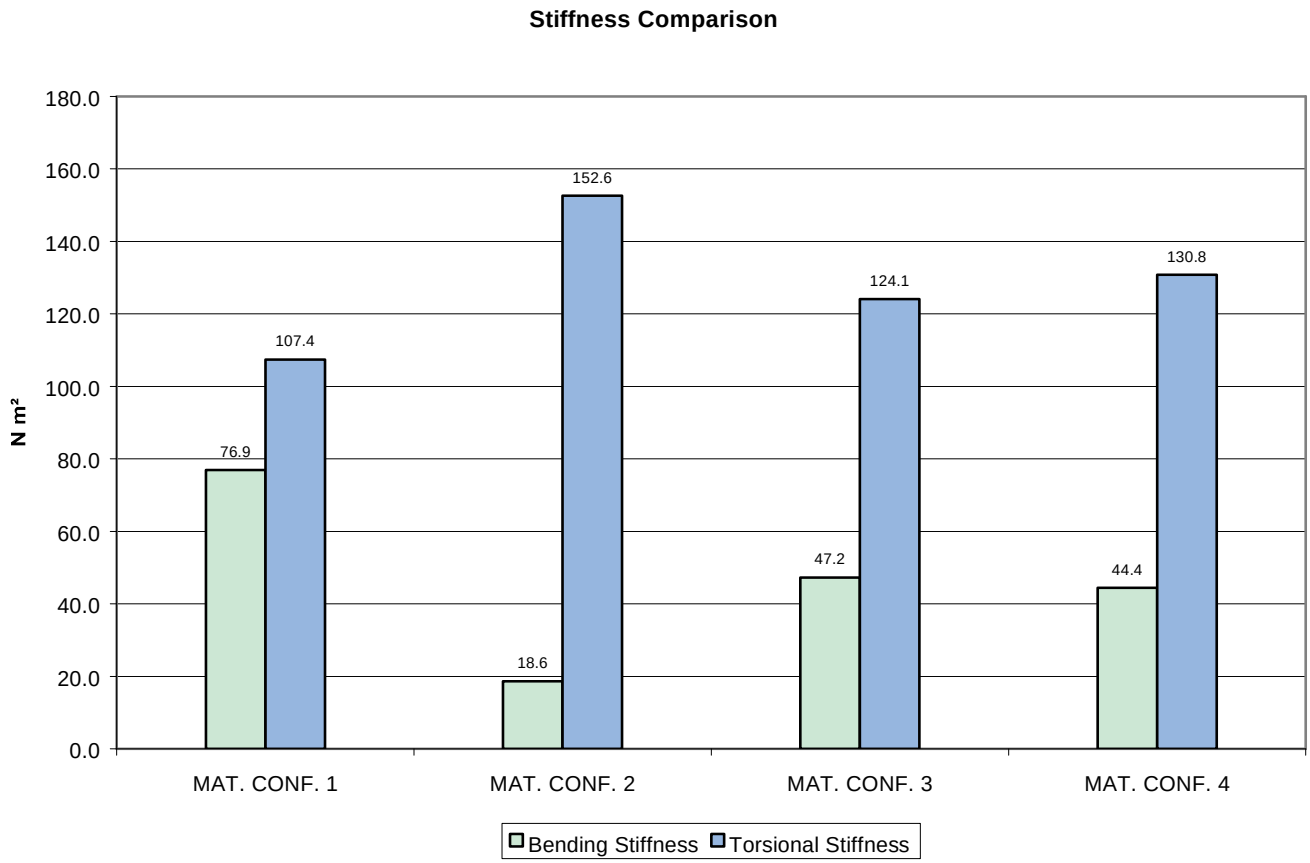

Figure 3 - Theoretical stiffness comparison.

The critical concern is the deflection of the silicon sensors due to gravitational loads and due to external loading, e.g. cooling line connections and cables. Staves will be mounted in all orientations so we have studied the deflections for staves oriented as shown in Figure 1 (horizontal configuration - X) and rotated 90 degrees (vertical configuration - Y).

Although a portion of the load is concentrated in the hybrid regions, we have modeled the stave load as uniform along the full length with a value of 2.1 N/m (0.012 lbs/in). Point loads were applied centered

between support points to simulate potential loads induced by cables at the hybrid location, or by handling during assembly. Finally, moment loads were applied to the ends of the staves, simulating effects of the cooling and cable connections from the staves to the outside world (unit loads were applied and one should scale the results as appropriate for realistic load estimates) or possible misalignment of the supports. Summarizing results are presented for three load cases

1. gravity
2. 4.9 N (~1.1 lbf) concentrated load half the way between two supports (equivalent to the load transmitted by a mass of 0.5 kg)
3. 0.113 N·m (1 lbf) torque at the stave ends

and assuming three different support conditions

1. simple support at each end;
2. fixed support at each end;
3. simple support at the middle and ends of the stave[1].

Configuration 4 (see Figure 2) provides the best overall behaviour in terms of stiffness and radiation length;it has been used for the deflection results presented in Figure 4, the stresses in the silicon in Figure 5 and the stresses in the composite shell structure in Figure 6. The first support case is typical of what may be experienced during assembly handling so the deflections are not a concern, but the stress levels are. To set the scale for the stresses, the published silicon yield stress is 120 MPa and that for the composites is around 1500-2200 MPa. For the silicon one should be careful as stress concentrations from defects along the cut edges can significantly increase the local stress above the nominal stresses presented in Figure 5, leading to failure under much lower load conditions than the naïve expectation. In this case the factors of safety are extremely generous and one would not anticipate any materials failures[2]. We do not think that the second support condition is realizable in the detector assembly, but present it for completeness. The third support condition is what we anticipate for the final mounting condition of the staves. Here it is the deflections that are critical. Figure 4 shows that the self-deflection is well under control at ~30 microns. The deflection due to

[1] In this case, for load condition 2, loads are applied at the midpoints of both of the unsupported spans.

[2] Cantilever support of the stave from one end will increase the stresses by a factor of 4, still well below any conceivable failure point. If, however, a partially assembled stave without the outer structure were to be simply supported from the ends the deflection would be around 50mm and the stress in the silicon would be about 15Mpa which may be a concern given the possibility of stress fractures originating from defects along the cut edges.

external loads of 4.9 N on each unsupported span should be scaled down by at least a factor of ten given the expected loading one might see in the as-installed condition.

Finally, it should be noted that the natural frequency of the staves (Figure 7) are closely related to the maximum deflection under self-loading[3]. For deflections above 50 microns the natural frequency is dropping into the 60Hz range, which we feel should be avoided. Therefore the maximum acceptable beam deflection is driven by the requirement of staying sufficiently far above a natural frequency of 60Hz rather than the maximum allowable for the required sensor alignment tolerances needed for the vertex trigger (~200 microns).

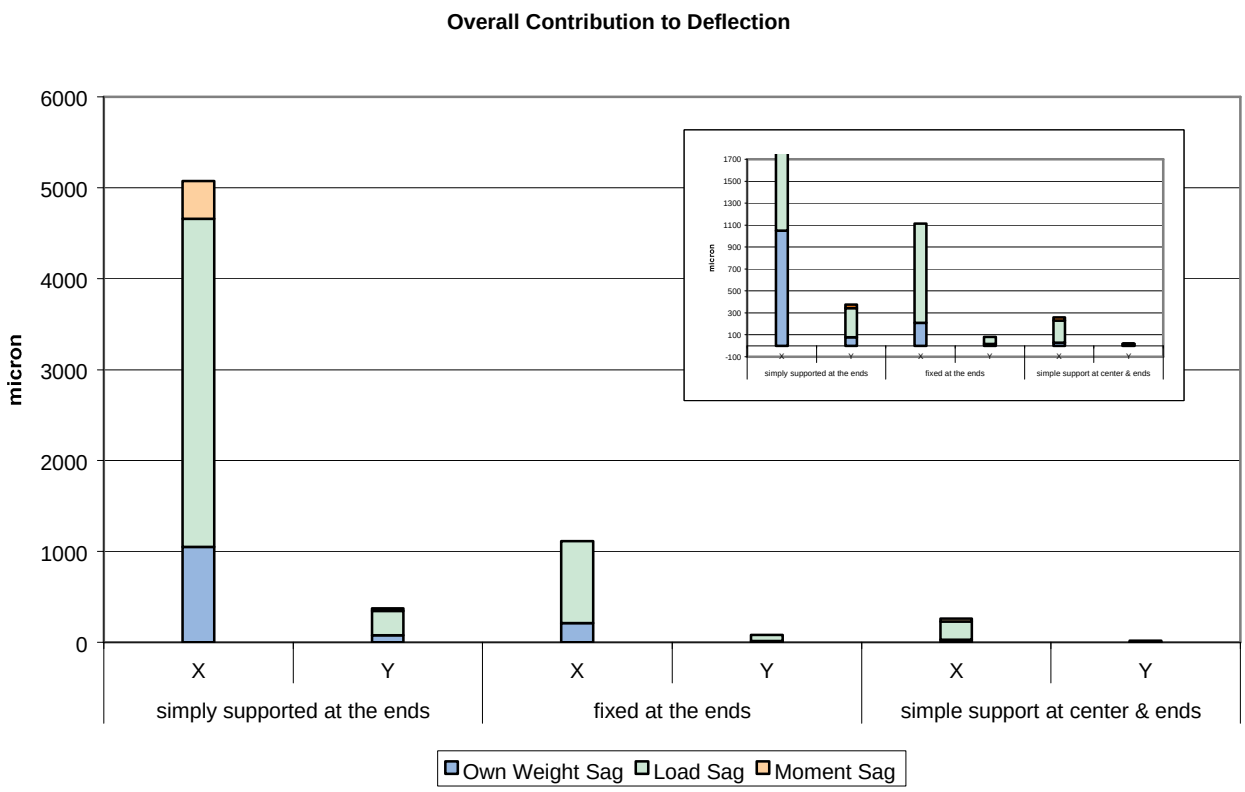

Figure 4 – Overall deflection

[3] The natural frequency is, to good approximation, directly proportional to the square root of the maximum deflection.

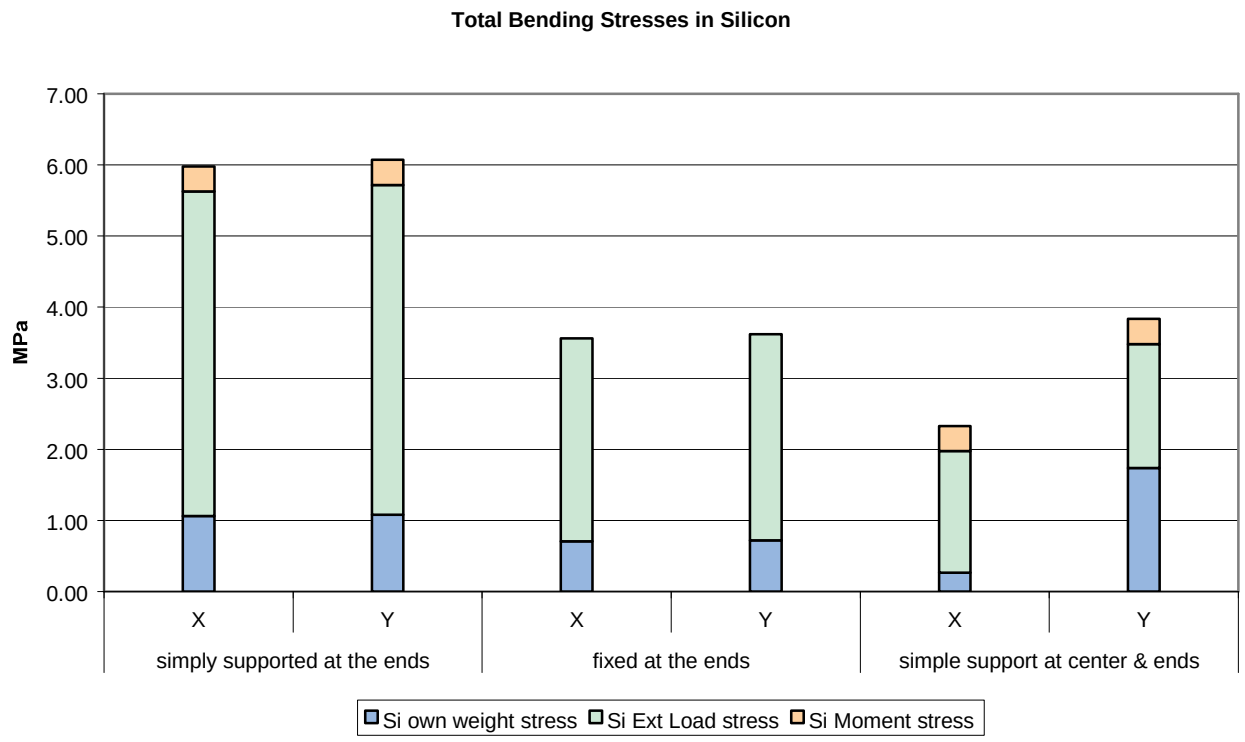

Figure 5 – Bending stresses in the silicon sensor

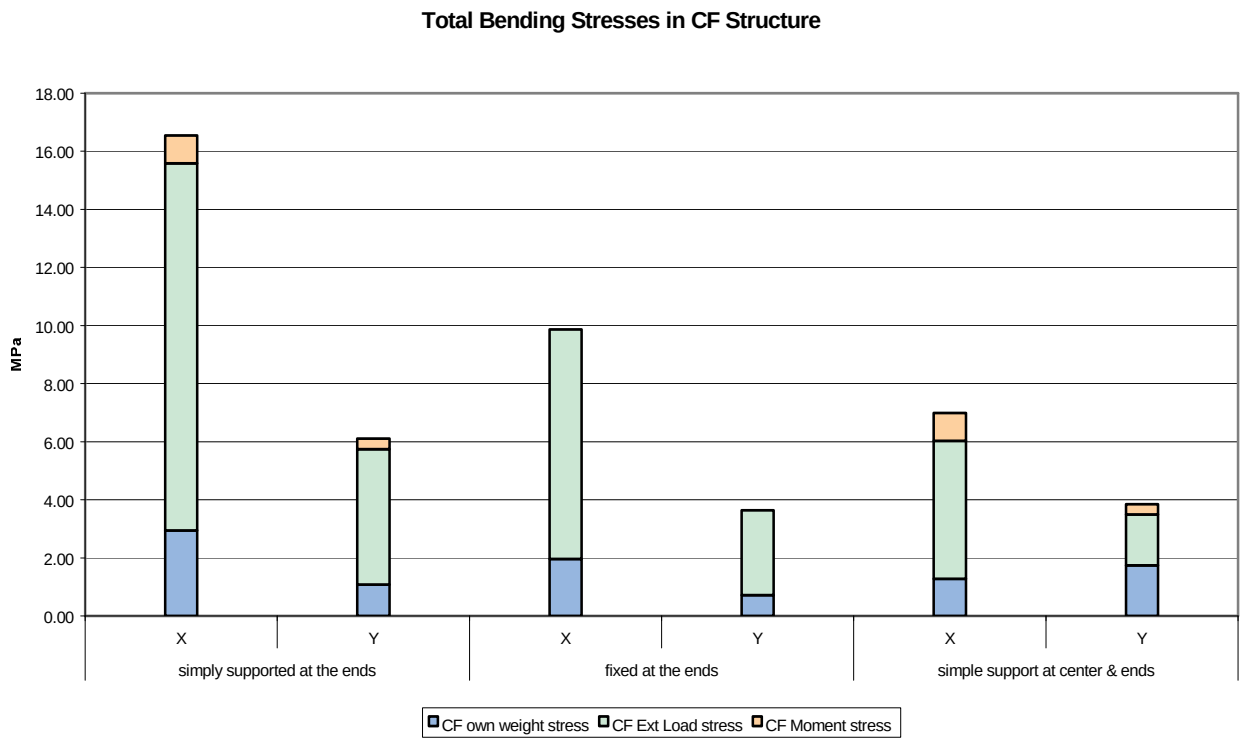

Figure 6 – Bending stresses in the carbon fiber structure

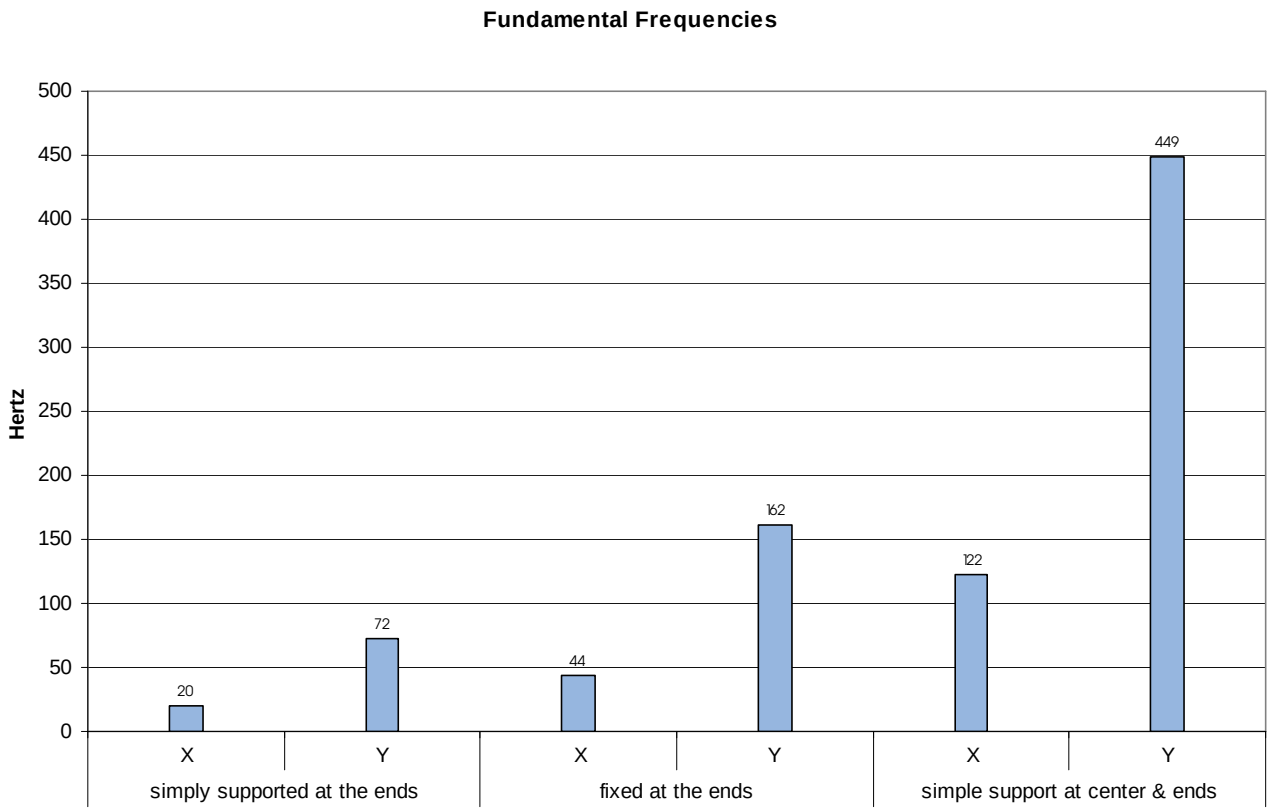

Figure 7 – Calculated stave fundamental frequencies

4.3. Finite element analysis

We consider, in addition to the theoretical investigation, a simple finite element model of the stave outer shell. The model has a longitudinal length of 10 mm with one end fully constrained around the perimeter. Two load cases are depicted in Figure 8: 1) a longitudinally distributed torque totaling 10 N·m and 2) two longitudinally distributed loads, totaling 20 N, applied along the edges of the stave. in The results of the FEA are shown in Figure 9 through Figure 16 and the displacements summarized in Table 7. Material configuration 4 provides the best torsional performance and a flexural behaviour comparable to the other configurations.

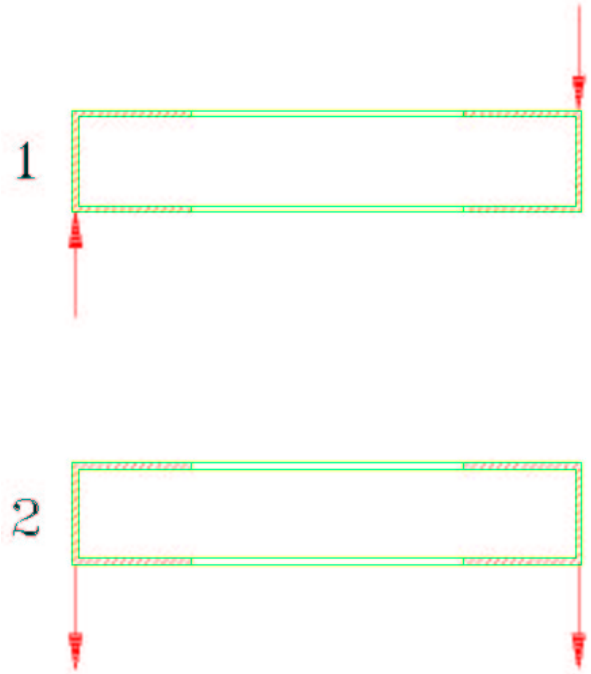

Figure 8 - Load Cases. Case 1: 10 N.m (~88.5 lbf in) torque distributed along the longitudinal length. Case 2: 10 N x 2 (~2.25 lbf x2) distributed along the longitudinal length

Configuration [material - load]	**min displacement** [μm]	**max displacement** [μm]
1-torsion	.1	13
1-flexure	0.2	0.8
2-torsion	0	17
2-flexure	0.3	1.1
3-torsion	0	13
3-flexure	0.2	0.8
4-torsion	1	11
4-flexure	0.3	0.8

Table 7 – Finite element analysis displacement summary.

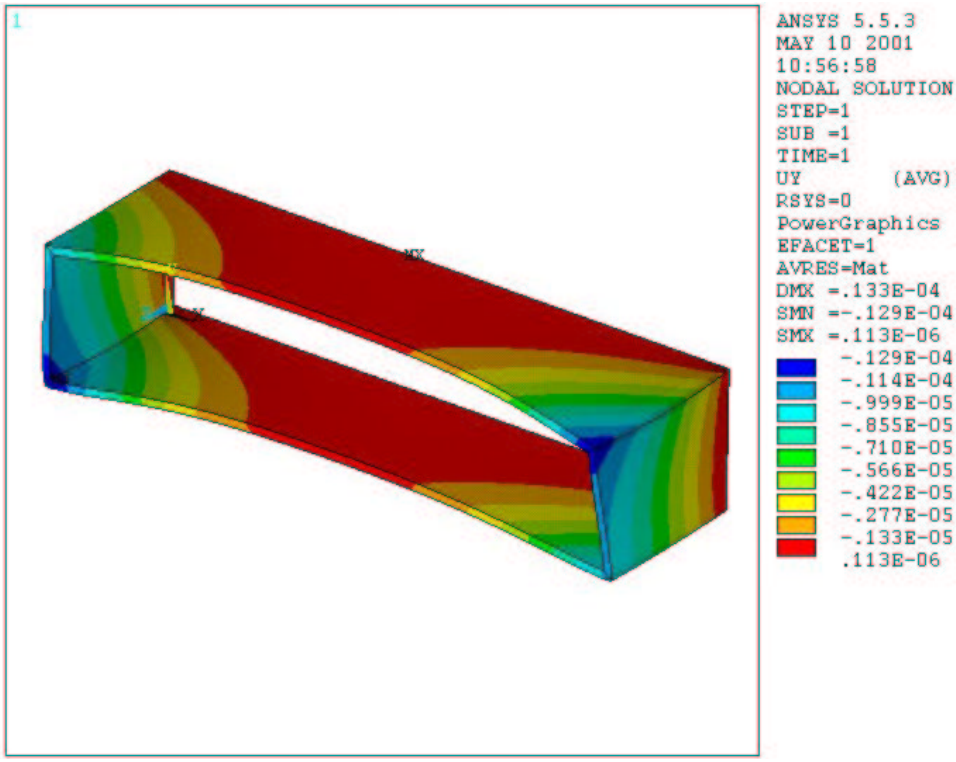

Figure 9 – Material Configuration 1, Load Case 1

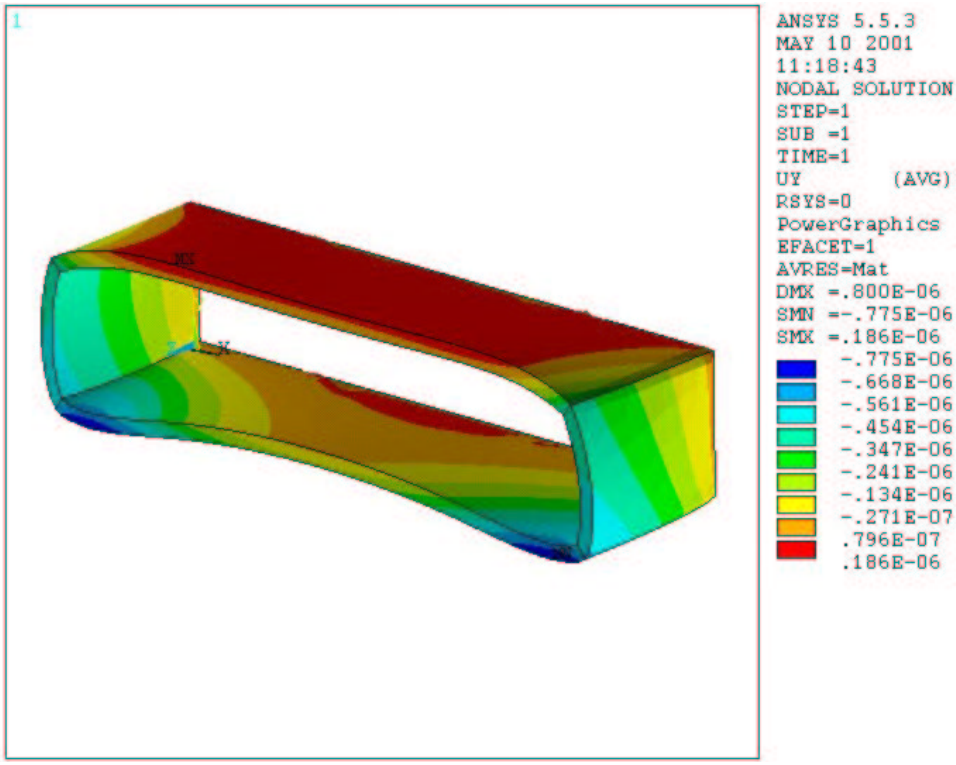

Figure 10 – Material Configuration 1, Load Case 2

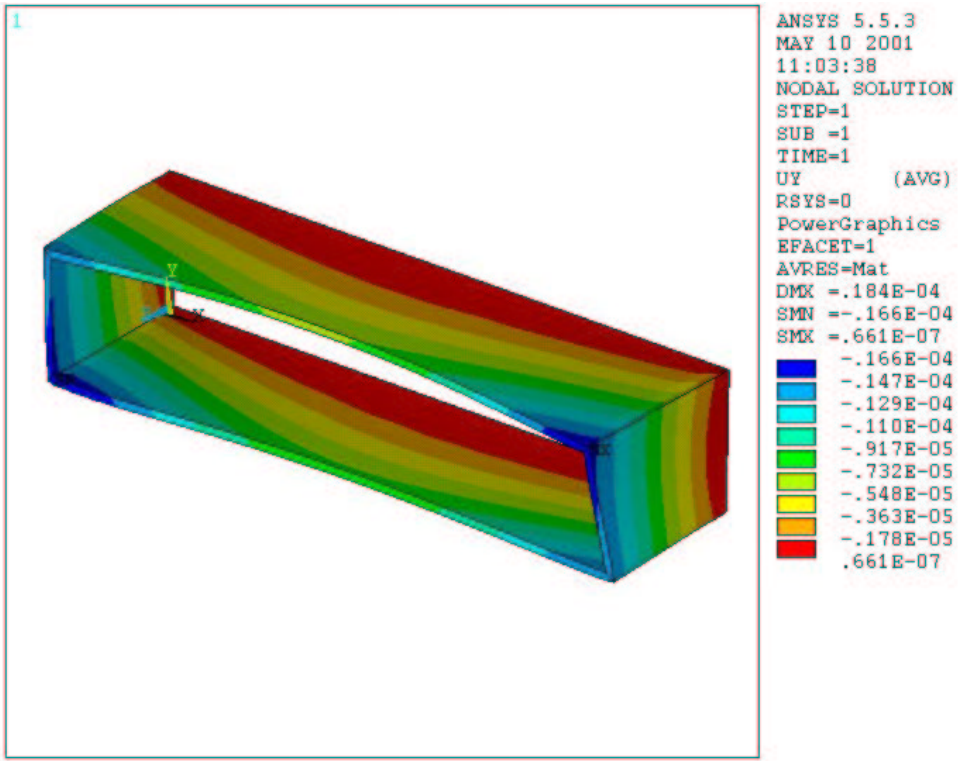

Figure 11 – Material Configuration 2, Load Case 1

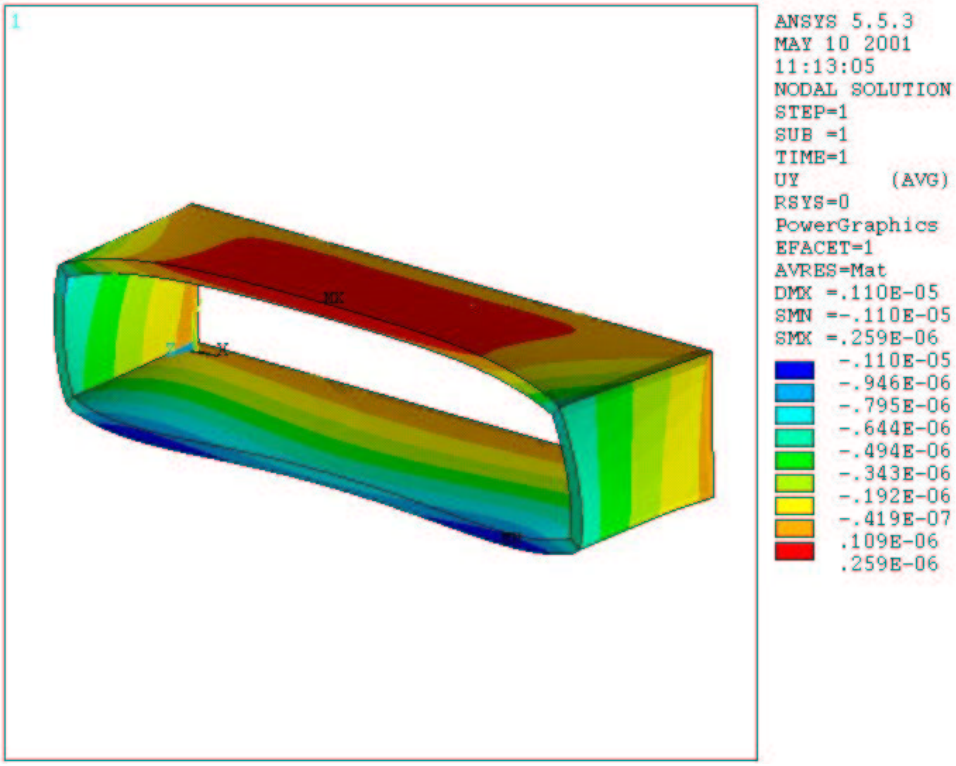

Figure 12 – Material Configuration 2, Load Case 2

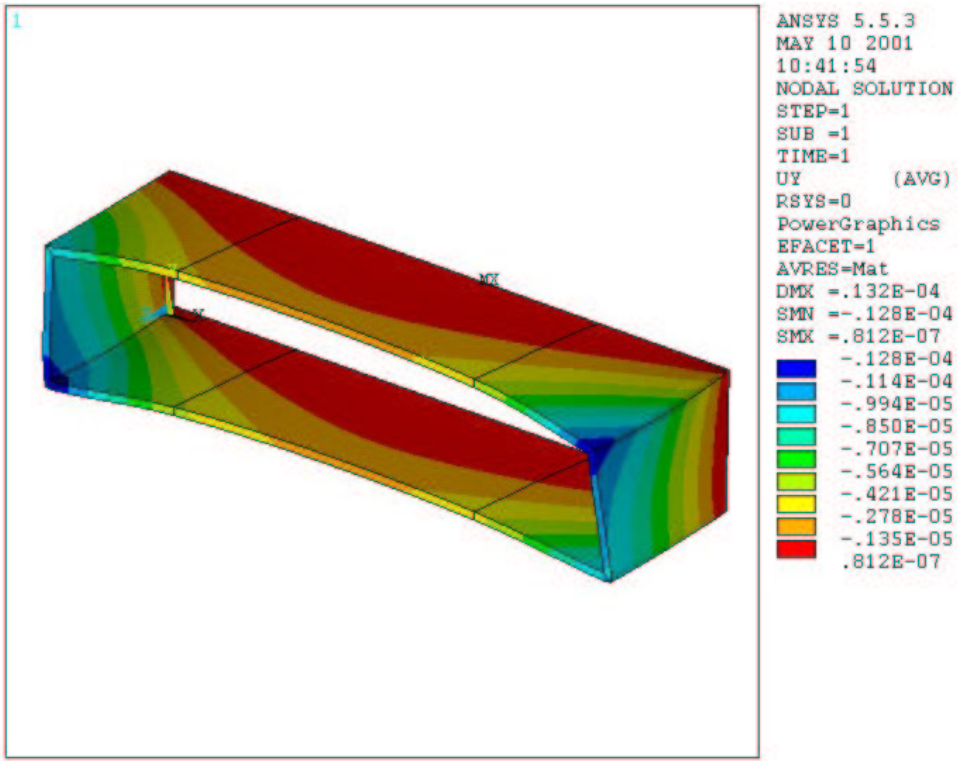

Figure 13 – Material Configuration 3, Load Case 1

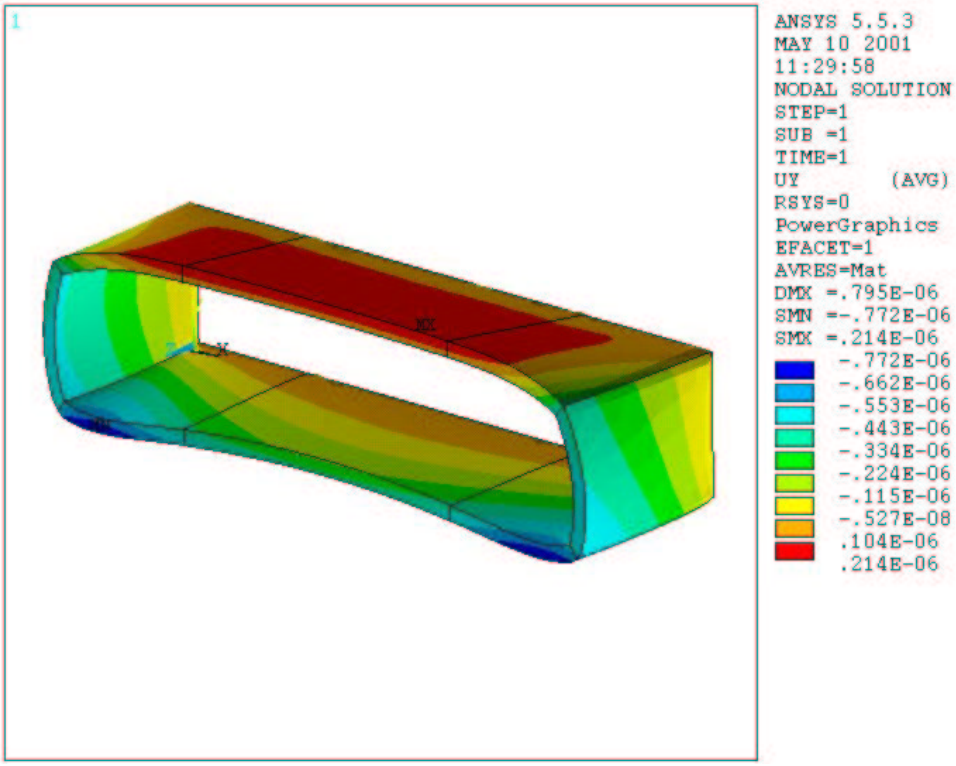

Figure 14 – Material Configuration 3, Load Case 2

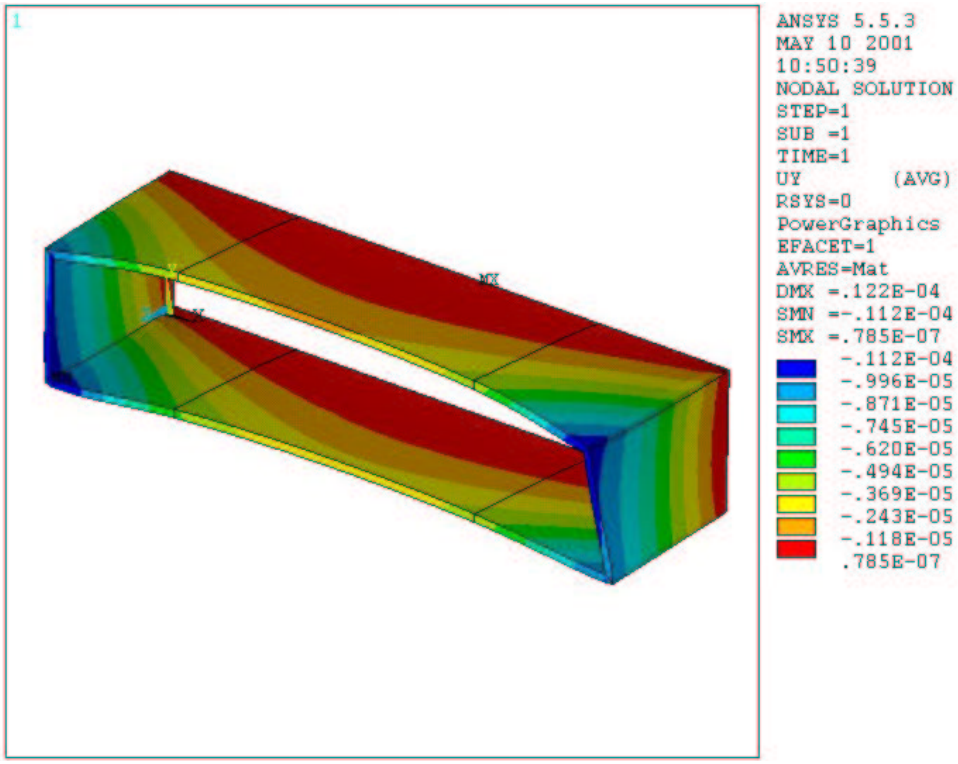

Figure 15 – Material Configuration 4, Load Case 1

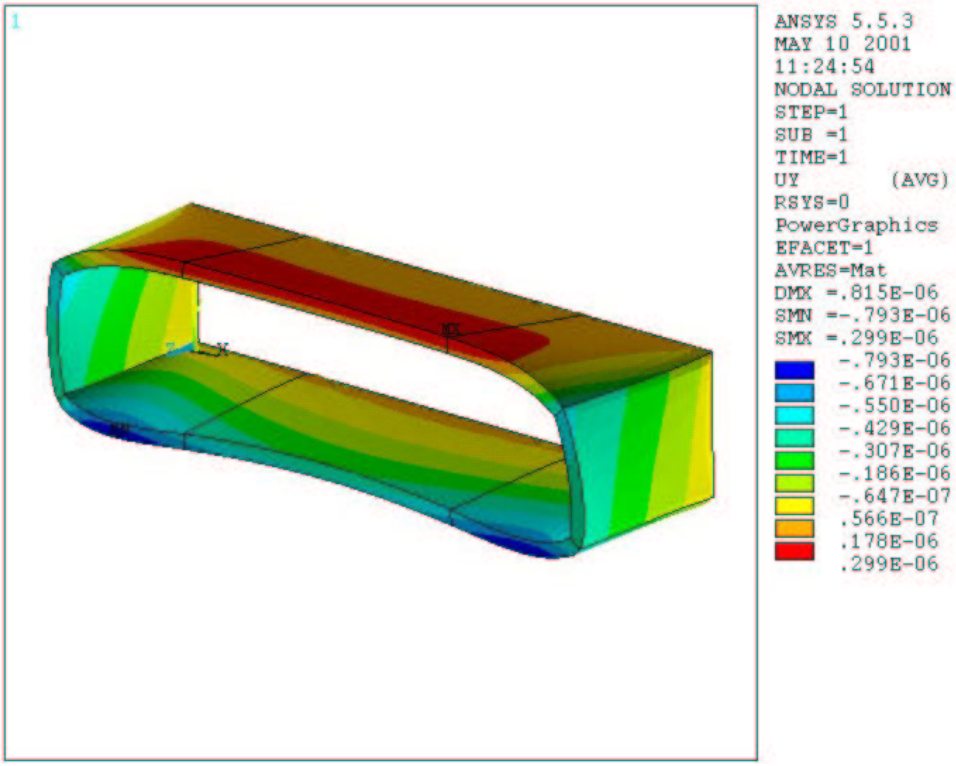

Figure 16 – Material Configuration 4, Load Case 2

5. Summary and conclusion

We have studied a proposed stave structure for the D0 Run IIb silicon detector outer layers. Several laminates have been proposed which closely match the thermal expansion coefficient of silicon. Only laminates that incorporate boron fibers can do so while maintaining significant stiffness along the long axis of the stave. The stave design achieves satisfactory stiffness for support at ~0.6m intervals. Prototypes should be fabricated and load tested to confirm these results and to investigate the effects of windows in the structure, required to allow for cable penetration and to reduce mass.

6. Appendix –spreadsheet used for theoretical analysis

D0 stave structural analysis

units: SI

	long cf	short cf	beam	silicon	peek	BeO***
b	43.18	0.50	4.76	37.20	6.00	35.00
h	0.25	8.64	1.78	0.30	2.00	0.50
xg	0.00	21.34	19.21	0.00	8.49	0.00
yg	4.20	0.00	0.00	1.15	0.00	1.43
Ix	190.03	26.87	2.24	14.84	1.18	35.90
Iy	1677.28	92.28	178.76	1286.97	119.18	1786.46
#. Pcs	2.00	2.00	2.00	2.00	2.00	10.00
Ix tot [mm**4]	380.05	53.75	4.47	29.69	2.36	359.01
Iy tot [mm**4]	3354.57	184.56	357.52	2573.94	238.36	17864.58
E [Gpa]	105.00	105.00	4.14	112.40	3.80	345.00
ρ [g/cc]	2.20	2.20	0.32	2.33	1.42	2.85
Load [N/m]	0.186	0.186	0.053	0.510	0.334	
EIx [N m**2]	39.91	5.64	0.02	3.34	0.01	
EIy [N m**2]	352.23	19.38	1.48	289.31	0.91	
Σ EIx	48.913		Σ EIy	663.304		
	0.217	coolant load [N/m]				
	0.158	cables [N/m]				

Length	1.2	m	
total distributed load	1.645	N/m	
substrate Load	0.245	N	
P chip	0.064	N	
concentrated loads	0.309	N	
equiv. Distr. Load	1.903	N/m	
Load [N]	4.905	N	
Moment [Nm]	0.113	Nm	
y max Si	1.350		18.600 mm
y max CF	4.000		20.000 mm

simply supported at the ends

Own Weight	X	Y				
max sag	1050	77	micron		l [m]	a [m]*
Ra & Rb	1.14		N		1.2	0.6
Max internal M @ x = a	0.34		Nm			
Max bending stress in silicon from M**	1.06	1.08	Nmm**2	{MPa}		
Max bending stress in CF from M	2.94	1.08	Nmm**2	{MPa}		
Si own weight stress	1.06	1.08	Nmm**2			
CF own weight stress	2.94	1.08	Nmm**2			
fundamental frequency	19.64	72.33	Hertz			

central LOAD				
max sag	3610	266	micron	
Ra & Rb	2.45		N	
Max internal M @ x = a	1.47		Nm	
Max bending stress in silicon from M**	4.56	4.64	Nmm**2	{MPa}
Max bending stress in CF from M	12.64	4.66	Nmm**2	{MPa}
Si LOAD stress	4.56	4.64	Nmm**2	{MPa}
CF LOAD stress	12.64	4.66	Nmm**2	{MPa}

Concentrated MOMENT at the ends					
max sag	416	31	micron	@	0.50718m
Ra [Rb = -Ra]	0.00		N		
Max internal M	0.11		Nm	constant along the beam	
Max bending stress in silicon from M**	0.35	0.36	Nmm**2	{MPa}	
Max bending stress in CF from M	0.97	0.36	Nmm**2	{MPa}	
Si MOMENT stress	0.35	0.36	Nmm**2	{MPa}	
CF MOMENT stress	0.97	0.36	Nmm**2	{MPa}	

fixed at the ends

Own Weight	X	Y				
max sag	210	15	micron		l [m]	a [m]*
Ra & Rb	1.14		N		1.2	0.6
Max internal + M @ x = a	0.11		Nm			
Max internal - M @ x = 0, L	-0.23		Nm			
Max bending stress in silicon from + M**	0.35	0.36	Nmm**2	{MPa}		
Max bending stress in silicon from - M**	0.71	0.72	Nmm**2	{MPa}		
Max bending stress in CF from +M	0.98	0.36	Nmm**2	{MPa}		
Max bending stress in CF from - M	1.96	0.72	Nmm**2	{MPa}		
Si own weight stress	0.71	0.72	Nmm**2			
CF own weight stress	1.96	0.72	Nmm**2			
fundamental frequency	43.92	161.72	Hertz			

Central LOAD

max sag	903	67	micron	
Ra & Rb	2.45		N	
Ma	-0.74		Nm	
Max internal + M @ x = a	0.92		Nm	
Max internal - M @ x = 0	-0.74		Nm	
Max bending stress in silicon from +M**	2.85	2.90	Nmm**2	{MPa}
Max bending stress in silicon from - M**	2.28	2.32	Nmm**2	{MPa}
Max bending stress in CF from +M	7.90	2.91	Nmm**2	{MPa}
Max bending stress in CF from - M	6.32	2.33	Nmm**2	{MPa}
Si LOAD stress	2.85	2.90	Nmm**2	{MPa}
CF LOAD stress	7.90	2.91	Nmm**2	{MPa}

Concentrated MOMENT at the ends

max sag	0	0	micron	
Ma, Mb	0		Nm	
Max internal M @ x = 0, L	0		Nm	
Max bending stress in silicon from - M**	0	0	Nmm**2	{MPa}
Max bending stress in CF from - M	0	0	Nmm**2	{MPa}
Si MOMENT stress	0	0	Nmm**2	{MPa}
CF MOMENT stress	0	0	Nmm**2	{MPa}

simple support at center & ends

Own Weight	X	Y				
max sag	27	2	micron	@	0.2529	m
Ra & Rb	0.43		N			
Rc	0.71		N			
Max internal + M @	0.05		Nm	@	0.225	m
Max internal - M @ x = L/2	-0.09		Nm			
Max bending stress in silicon from +M**	0.15	0.15	Nmm**2	{MPa}		
Max bending stress in silicon from - M**	0.27	0.27	Nmm**2	{MPa}	l [m]	a [m]*
Max bending stress in CF from +M	1.28	0.15	Nmm**2	{MPa}	0.6	0.3
Max bending stress in CF from - M	0.74	0.27	Nmm**2	{MPa}		
Si own weight stress	0.27	1.74	Nmm**2			
CF own weight stress	1.28	1.75	Nmm**2			
fundamental frequency	121.93	449.01	Hertz			

Central LOAD

max sag	202	15	micron	@	0.27	m
Ra & Rb	1.53		N			
Rc	3.37		N			
Mc	0.55		Nm			
Max internal + M @ x = a	0.46		Nm			
Max internal - M (@ x = L/2	-0.55		Nm			
Max bending stress in silicon from +M**	1.43	1.45	Nmm**2	{MPa}		
Max bending stress in silicon from - M**	1.71	1.74	Nmm**2	{MPa}		
Max bending stress in CF from +M	3.95	1.46	Nmm**2	{MPa}		
Max bending stress in CF from - M	4.74	1.75	Nmm**2	{MPa}		
Si LOAD stress	1.71	1.74	Nmm**2	{MPa}		
CF LOAD stress	4.74	1.75	Nmm**2	{MPa}		

Concentrated MOMENT at the ends

max sag	31	2	micron	@	0.2m
Ra & Rb	-0.28		N		
Rc	0.57		N		
Max internal + M @ x = 0, L	0.11		Nm		
Max bending stress in silicon from +M**	0.35	0.36	Nmm**2	{MPa}	
Max bending stress in CF from +M	0.97	0.36	Nmm**2	{MPa}	
Si MOMENT stress	0.35	0.36	Nmm**2	{MPa}	
CF MOMENT stress	0.97	0.36	Nmm**2	{MPa}	

NOTES

* a is half the distance between supports
**compare to 120 MPa Compressive Yield Strength & 586 MPa Max Tensile Strength for Si
and 2.93 GPa Compressive Yield Strength, 1.5GPa Max Tensile Strength, 1.8 GPa Max Flexural Strength for Boron CF
*** 50mm long in z (it is not kept into account as a structural member)